energies

MDPI

Article

Design and Implementation of Robust $H\infty$ Control for Improving Disturbance Rejection of Grid-Connected Three-Phase PWM Rectifiers

Naima Ait Ramdane [1,2], Adel Rahoui [2,3], Boussad Boukais [2], Mohamed Fouad Benkhoris [1,*], Mourad Ait-Ahmed [1] and Ali Djerioui [1,4]

1 IREENA Laboratory, University of Nantes, 44602 Saint-Nazaire, France; naima.aitramdane@ummto.dz (N.A.R.); mourad.ait-ahmed@univ-nantes.fr (M.A.-A.); ali.djerioui@univ-msila.dz (A.D.)
2 L2CSP Laboratory, Mouloud Mammeri University of Tizi-Ouzou, BP 17 RP, Tizi-Ouzou 15000, Algeria; a.rahoui@enstp.edu.dz (A.R.); boussad.boukais@ummto.dz (B.B.)
3 Ecole Nationale Supérieure des Travaux Publics Francis Jeanson, Rue Sidi Garidi BP 32 Vieux Kouba, Algiers 16051, Algeria
4 LGE Laboratory, Department of Electrical Engineering, Mohamed Boudiaf University of M'Sila, BP 166 Ichbilia, M'Sila 28000, Algeria
* Correspondence: mohamed-fouad.benkhoris@univ-nantes.fr

Abstract: In response to the high performance requirements of pulse width modulation (PWM) converters in grid-connected power systems, H-Infinity ($H\infty$) control has attracted significant research interest due to its robustness against parameter variations and external disturbances. In this work, an advanced robust $H\infty$ control is proposed for a grid-connected three-phase PWM rectifier. A two-level control strategy is adopted, where cascaded $H\infty$ controllers are designed to simultaneously regulate the DC bus voltage and input currents even under load disturbances and non-ideal grid conditions. As a result, unit power factor, stable DC bus voltage, and sinusoidal input currents with lower harmonics can be accurately achieved. The design methodology and stability of the proposed controller are verified through a comprehensive analysis. Simulation tests and experimental implementation on a dSPACE 1103 board demonstrate that the proposed control scheme can effectively enhance disturbance rejection performance under various operating conditions.

Keywords: disturbance rejection; H-infinity control; robust control; three-phase pulse width modulation (PWM) rectifier; unbalanced grid voltage

Citation: Ait Ramdane, N.; Rahoui, A.; Boukais, B.; Benkhoris, M.F.; Ait-Ahmed, M.; Djerioui, A. Design and Implementation of Robust $H\infty$ Control for Improving Disturbance Rejection of Grid-Connected Three-Phase PWM Rectifiers. *Energies* **2024**, *17*, 2166. https://doi.org/10.3390/en17092166

Academic Editor: Ahmed Abu-Siada

Received: 2 April 2024
Revised: 24 April 2024
Accepted: 30 April 2024
Published: 1 May 2024

1. Introduction

In recent decades, three-phase pulse width modulation (PWM) voltage source converters (VSCs) have received a lot of attention in electrical power conversion systems due to their high reliability and security [1–4]. The VSCs can operate either as a rectifier or inverter. Grid-connected three-phase PWM rectifiers are an ideal choice among different power quality improved rectifiers. The attractive features of these rectifiers are better control of dc voltage, nearly unity power factor operation and less harmonic content in grid current [5]. They are used in various industrial power applications, including, uninterruptable power supplies (UPSs), variable speed wind generators, high-voltage direct-current (HVDC) transmission systems, electric vehicle charging systems, rail traction supply systems, energy storage systems, grid power factor correction, active filters and other fields [6–11].

Commonly, grid-connected three-phase PWM rectifiers facilitate multiple control loops to achieve different control objectives. A phase-locked loop (PLL) is used for grid synchronization; a current control loop is used for current control and fast current limitation; an active power control loop is used for active power tracking; and a voltage control loop is used to regulate the dc bus voltage [12]. The most commonly used control topologies are the direct power control (DPC) [13–18] and voltage-oriented control (VOC) [19–23]. These methods use the concept of decoupled active and reactive power control, which is realized in the synchronous reference frame (SRF). The DPC technique is based on p-q theory [24] where instantaneous power errors of active and reactive power components are kept within a fixed hysteresis band to provide reference values of powers. However, the behavior of hysteresis regulators causes a variable frequency switching pattern of the semiconductor devices used in the converter [25]. In the VOC method, the ac side currents are transformed into active and reactive components and compared with reference currents in order to eliminate the error between the reference and measured values of the active and reactive powers. The proportional integral (PI) controllers are used to track the reference. Fine-tuning of PI controllers is necessary to get a satisfactory steady and dynamic response. Moreover, in order to address the non-linear nature of PWM rectifiers, various studies [26–29] propose a dual closed-loop control strategy with an outer-loop controlling square of DC voltage and inner-loop controlling AC current.

Usually, the mentioned methods are designed assuming ideal conditions, while recent studies have focused on improving their performance under unbalanced grid conditions, load disturbances and parametric uncertainties. In this regard, numerous scholars have proposed various control strategies, including adaptive controllers [30], fuzzy controllers [31], fractional-order controllers [5,32], sliding mode control [26,33], predictive control [2,34], adaptive neural network (ANN) structure control [2], and H-Infinity ($H\infty$) control [35–40].

One convenient approach to achieve optimal performance under load disturbances and parametric uncertainties is to use $H\infty$ robust controllers. In [35], an optimal voltage control problem was addressed for islanded power converters using $H\infty$ synthesis. Similarly, in [36], $H\infty$ synthesis was employed to enhance the robustness of the converter's output current controller against varying grid impedance. Additionally, for harmonic suppression, $H\infty$ control was explored in [37] to design output voltage controllers capable of rejecting harmonic disturbances from nonlinear loads or the public grid. In microgrid applications, both $H\infty$ and gain scheduled $H\infty$ controllers were utilized for robust control, as discussed in [38,39]. Recently, in [40], $H\infty$ loop shaping is proposed to provide good stabilization and reference tracking for single-phase PWM rectifiers in the presence of current sensor gain faults. Although the cited strategies provide satisfactory results, some of them involve the development of multiple-input multiple-output (MIMO) $H\infty$ controllers, which inherently introduce increased complexity in controller design and implementation [37,41]. On the other hand, the majority of proposed $H\infty$ control strategies are applied for the inner loop of PWM rectifiers, where the outer loop is generally controlled using proportional integral (PI) controllers [40,42,43]. However, these controllers are less robust as they may struggle to maintain stability and performance in the presence of significant disturbances or uncertainties in the system.

To address the previously cited issues, a robust $H\infty$-based control scheme is proposed to enhance power quality in grid-connected three-phase PWM VSCs, under unbalanced grid voltage and constrained load conditions. A two-level control approach using cascaded $H\infty$ controllers is introduced to simultaneously regulate DC bus voltage and input currents. This method is based on a linearized model of the converter, which is decomposed into two single-input single-output (SISO) systems. This decomposition results in a simpler controller structure with reduced order and ease of implementation compared to MIMO-based controllers. Additionally, introducing an $H\infty$ controller for DC bus voltage regulation enhances convergence speed and reduces overshoots of the outer loop during disturbances. Experimental tests are presented to assess the performance and robustness of the proposed controller under various conditions, including unbalanced grid voltage and load variations.

The remainder of this paper is organized as follows: In Section 2, the dynamic model of the system including the grid utility, a three-phase PWM rectifier and a variable DC load is presented. Section 3 provides a general overview of the $H\infty$ control basic principle. Section 4 details the design of the proposed cascaded $H\infty$-based control and analyzes the controller's dynamic performance through experimental tests. Experimental results that demonstrate the effectiveness of the control scheme under various test conditions are presented in Section 5. Section 6 concludes this article.

2. System Description and Modeling

The configuration of the studied system is shown in Figure 1. A three-phase PWM rectifier is connected to the grid through a passive L filter, while a DC load R_L is connected across the DC-link capacitor C.

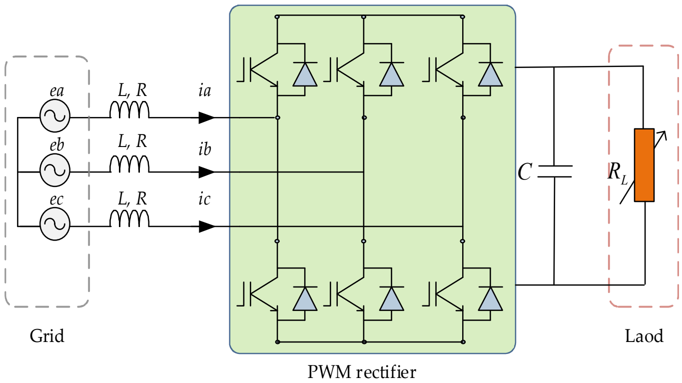

Figure 1. Grid-connected rectifier scheme.

The dynamical model of the PWM rectifier can be expressed in the *abc* reference frame as follows:

$$\frac{d}{dt}\begin{bmatrix} i_a \\ i_b \\ i_c \end{bmatrix} = \frac{R}{L}\begin{bmatrix} i_a \\ i_b \\ i_c \end{bmatrix} + \frac{1}{L}\left(\begin{bmatrix} v_a \\ v_b \\ v_c \end{bmatrix} - \begin{bmatrix} e_a \\ e_b \\ e_c \end{bmatrix}\right) \tag{1}$$

$$C\frac{d}{dt}V_{dc} = S_a i_a + S_b i_b + S_c i_c - \frac{V_{dc}}{R_L} \tag{2}$$

where e_a, e_b and e_c represent the grid voltages, i_a, i_b and i_c are the AC-line currents, and v_a, v_b and v_c are the rectifier input voltages. S_a, S_b and S_c denote the switching states of three insulated-gate bipolar transistors (IGBTs) in the upper bridge legs. L and R are, respectively, the inductance and resistance of the AC filter.

In this study, the VOC is employed to regulate the AC-line currents. Consequently, the control is executed in the *dq* reference frame. The PWM rectifier model in the *dq* reference frame is expressed as follows:

$$\frac{d}{dt}\begin{bmatrix} I_d \\ I_q \end{bmatrix} = \begin{bmatrix} -R/L & -\omega \\ \omega & -R/L \end{bmatrix}\begin{bmatrix} I_d \\ I_q \end{bmatrix} + \frac{1}{L}\begin{bmatrix} V_d \\ V_q \end{bmatrix} - \frac{1}{L}\begin{bmatrix} E_d \\ E_q \end{bmatrix} \tag{3}$$

$$C\frac{d}{dt}V_{dc} = \frac{3}{2}\left(S_d i_d + S_q i_q\right) - \frac{V_{dc}}{R_L} \tag{4}$$

where E_d, E_q, I_d and I_q are, respectively, the d- and q-axis components of the grid voltages and AC-line currents; V_d and V_q are the d- and q-axis components of the rectifier input voltages. S_d and S_q denote the switching states d- and q-axis components of the IGBTs in the upper bridge legs.

The AC side rectifier active power P_G is given by:

$$P_G = E_d I_d + E_q I_q. \tag{5}$$

By setting the grid voltage E_d component to zero through a phase-locked loop (PLL) [44], a simplified expression for P_G can be derived as follows:

$$P_G = E_q I_q. \tag{6}$$

On the rectifier's DC side, the modeling of the DC-link voltage dynamics involves considering a pure capacitor. As a result, the power P_{dc} obtained from stored electrical energy can be expressed as follows:

$$P_{dc} = \frac{d}{dt}\left(\frac{1}{2}CV_{dc}^2\right) = P_G - P_L \tag{7}$$

where $P_L = V_{dc}^2/R_L$ is the power at the DC side of the rectifier (load).

From (7), it can be deduced:

$$P_G = \frac{1}{2}C\frac{d}{dt}V_{dc}^2 + \frac{V_{dc}^2}{R_L}. \tag{8}$$

The following equation can be derived from (6) and (8):

$$E_q I_q = \frac{1}{2}C\frac{d}{dt}V_{dc}^2 + \frac{V_{dc}^2}{R_L}. \tag{9}$$

To facilitate the controller design, the aforementioned expression is reformulated by considering a fictitious variable where $\widetilde{V}_{dc} = V_{dc}^2$. Accordingly, the nonlinear DC voltage dynamics can be assimilated to an equivalent linear system, on which traditional linear controller design methods can be applied. Equation (9) becomes:

$$E_q I_q = \frac{1}{2}C\frac{d}{dt}\widetilde{V}_{dc} + \frac{\widetilde{V}_{dc}}{R_L}. \tag{10}$$

3. *H*∞ Control Principle

Figure 2 illustrates the standard control configuration wherein the nominal plant and the weighting functions are integrated to establish a closed-loop system. This leads to an augmented plant $P(s)$ with an exogenous input w that encompasses disturbance d, reference r, and noise signals n [42,45].

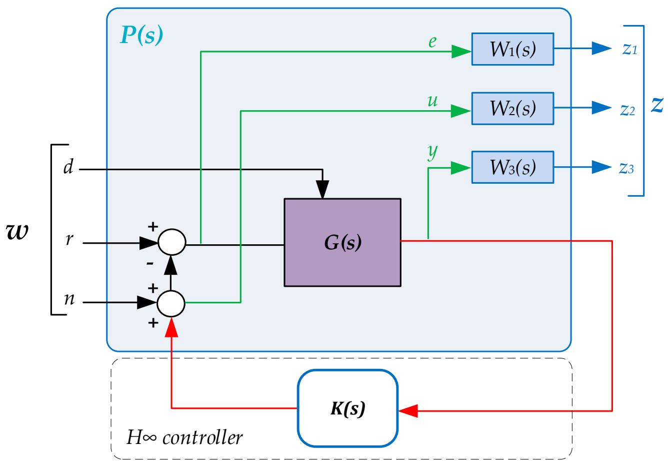

Figure 2. Weighted H-infinity control feedback structure.

Significant advancements have been achieved in $H\infty$ control synthesis since the pioneering works of G. Zames [45]. $H\infty$ control requires designing an optimal controller $K(s)$ for a nominal plant, ensuring that the $H\infty$ norm of the transfer function from the input w to the controlled output remains a bounded gain. This guarantees stability of the closed-loop system. The input information for the controller is incorporated into the augmented plant $P(s)$, as described in (11). This plant summarizes the dynamics of the open-loop system, the structure of the controller, and the control objectives and constraints. $P(s)$ is defined as follows:

$$P(s) = \begin{bmatrix} P_{zw}(s) & P_{zu}(s) \\ P_{vw}(s) & P_{vu}(s) \end{bmatrix}. \tag{11}$$

The generalized plant composed by different transfer functions from (w, u) to (z, y) is described as follows:

$$\begin{bmatrix} z(s) \\ y(s) \end{bmatrix} = \begin{bmatrix} P_{zw}(s) & P_{zu}(s) \\ P_{vw}(s) & P_{vu}(s) \end{bmatrix} \begin{bmatrix} w(s) \\ u(s) \end{bmatrix} \tag{12}$$

where $y(s)$ represents the measured output signals, and $z(s)$ the controlled outputs.

The relation between w and z can be expressed as follows [42,43]:

$$\begin{aligned} Z(s) &= F(P(s), K(s))\, W(s) \\ &= \left[P_{zw}(s) + P_{zu}(s)K(s)(I - P_{vu}(s)K(s))^{-1}P_{vw}(s)\right] W(s) \end{aligned} \tag{13}$$

where $F(P(s), K(s))$ is a linear fractional transformation, and I is the identity matrix.

3.1. Control Problem Formulation

The $H\infty$ control problem for the linear time-invariant system $G(s)$ with state space realization involves finding a specific matrix K (representing a static output feedback law, i.e., $u = Ky$) such that the $H\infty$ norm of $F(P(s), K(s))$ is constrained by a constant γ, which represents the desired performance level of the closed-loop system. This problem can be solved using either Ricatti equations or Linear Matrix Inequalities [46,47].

$$\|F(P(s), K(s))\, W(s)\|_{\infty} < \gamma. \tag{14}$$

Ultimately, the aim of the $H\infty$ control approach is to create a closed-loop system possessing strong robustness properties. At the core of this widely embraced concept lies the well know Small Gain Theorem, which stipulates that a stability sufficient condition for the closed-loop system is:

$$\|Tzw\|_{\infty} < 1. \tag{15}$$

3.2. Mixed Sensitivity Formulation

As previously mentioned, in $H\infty$ control theory, the controller is synthesized by optimizing the $H\infty$ norm of the cost function (Tzw). In the case of mixed sensitivity formulation, a transfer function from the exogenous input w to the performance output is filtered using weighting functions W_i (W_1, W_2, W_3). Then, the normalized augmented plant P is built from the nominal model G and weighting matrices W_i as follows [41].

$$\begin{bmatrix} Z_1 \\ Z_2 \\ Z_3 \\ e \end{bmatrix} = \begin{bmatrix} W_1 & -W_1G \\ 0 & W_2 \\ 0 & W_3G \\ I & -G \end{bmatrix} \begin{bmatrix} w \\ u \end{bmatrix}. \tag{16}$$

Based on Equation (16), the state space realization for $P(s)$ can be expressed as:

$$P(s) = \begin{bmatrix} A & B_1 & B_2 \\ C_1 & D_{11} & D_{12} \\ C_2 & D_{21} & D_{22} \end{bmatrix} = \begin{bmatrix} W_1 & -W_1G \\ 0 & W_2 \\ 0 & W_3G \\ I & -G \end{bmatrix}. \tag{17}$$

Let us assume that $P(s)$ satisfies the following assumptions:

1. (A, B_2) is stabilizable and (C_2, A) is detectable;

2. $D_{12} = \begin{bmatrix} 0 & 0 & 1 & 0 \\ 0 & 0 & 0 & 1 \end{bmatrix}^T$; $D_{21} = \begin{bmatrix} 0 & 0 & 0 & 0 \\ 0 & 0 & 0 & 0 \end{bmatrix}$ *and* $D_{22} = \begin{bmatrix} 0 & 0 \\ 0 & 0 \end{bmatrix}$;
3. $\begin{bmatrix} A - j\omega l & B_2 \\ C_1 & D_{12} \end{bmatrix}$ has a full column rank for ω;
4. $\begin{bmatrix} A - j\omega l & B_1 \\ C_2 & D_{21} \end{bmatrix}$ has a full row rank for ω.

A mixed sensitivity problem can be derived as follows:

$$P(s) = \begin{bmatrix} W_1 S \\ W_2 KS \\ W_3 T \end{bmatrix} \tag{18}$$

where $S = (I + GK)^{-1}$ is the sensitivity function, and $T = GK\,(I + GK)^{-1}$ is the complementary sensitivity function.

In the case of a mixed sensitivity problem, the objective is to find a rational function controller $K(s)$ that stabilizes the closed-loop system while satisfying the following expression:

$$\min\|P\| = \min \begin{bmatrix} W_1 S \\ W_2 KS \\ W_3 T \end{bmatrix} = \gamma. \tag{19}$$

The constant γ is defined as the minimum value to maintain system stability. The above-mentioned weighting functions are chosen to limit the sensitivity matrix, the control energy matrix, and the complementary sensitivity matrix of the controlled system. Applying the minimum gain theorem makes the H_∞ norm of $P(s)$ less than unity:

$$\left\| \begin{matrix} W_1 S \\ W_2 KS \\ W_3 T \end{matrix} \right\|_\infty < 1. \tag{20}$$

The H_∞ norm of P(s) is also the H_∞ norm of the cost function (Tzw):

$$\|Tzw\|_\infty = \left\| \begin{matrix} W_1 S \\ W_2 KS \\ W_3 T \end{matrix} \right\|_\infty < 1. \tag{21}$$

In this case, if $\|Tzw\|_\infty < 1$, then the desired robust performance specifications are satisfied. In $H\infty$ control design, the objective is to identify a stabilizing controller $K(s)$ that minimizes the $H\infty$ norm of Tzw while simultaneously optimizing the performance specifications. Therefore, the $H\infty$ control problem can be described as follows [41]:

$$\begin{gathered} \|F(P(s), K(s)),\, W(s)\|_\infty < \gamma \\ \min K\,\text{stabilising}\,P\|F(P(s), K(s)),\, W(s)\|_\infty = \min K\,\text{stabilising}\,P\|Tzw\|_\infty. \end{gathered} \tag{22}$$

According to (22), the controller function $K(s)$ can be obtained using γ iteration, which involves an internal optimization process to minimize $\|Tzw\|_\infty$.

4. Proposed $H\infty$ Cascaded Control Loops Design

The configuration of the proposed $H\infty$ control structure is illustrated in Figure 3. A dual-loop control scheme using $H\infty$ control is proposed to achieve robust control performance. It consists of a cascaded control scheme including two control loops: an inner loop and an outer loop. The inner controller $Kc(s)$ ensures the regulation of the input currents' dq components. The outer controller $Kv(s)$ ensures the control of the DC link voltage.

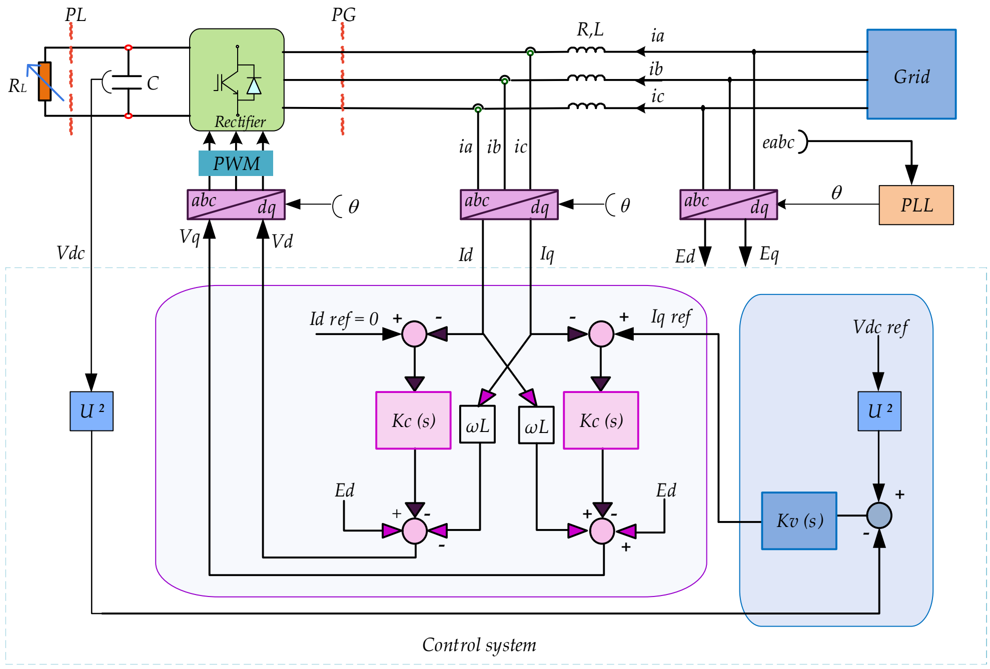

Figure 3. Proposed cascaded $H\infty$ control structure.

As mentioned above, the inner control loop regulates the AC-line current based on the VOC strategy. Furthermore, decoupling terms are included to separate the control of the q-axis and d-axis current components. The outer control loop regulates the DC-link voltage and calculates the q-axis current reference $I_{q,ref}$. In this regard, to obtain decoupled variables, the following representation is adopted, where the nominal control model includes the transfer matrices of the variables to be controlled, namely $G_{Idqnom}(s)$ and $G_{\tilde{V}dcnom}(s)$. After decoupling, the system can be expressed as follows:

$$\begin{bmatrix} G_{Idq,nom}(s) & 0 \\ 0 & G_{\tilde{V}dc,nom}(s) \end{bmatrix} = \begin{bmatrix} \frac{-1/R}{1+(L/R)s} & 0 \\ 0 & \frac{R_L}{1+(R_L C/2)s} \end{bmatrix}. \tag{23}$$

4.1. State Space Realization Models of Control Loops

The state space control loops models are used to obtain a state model of the PWM rectifier. where x $(x = x_c\ ;\ x = x_v), \in \mathbb{R}^n$ is the state vector; $w \in \mathbb{R}^{m_1}$ is the exogenous input vector; $u \in \mathbb{R}^{m_2}$ is the control input vector; $Z \in \mathbb{R}^{p_1}$ is the error vector and $y \in \mathbb{R}^{p_2}$, is the measurement vector, with $p_1 \geq m_2$ and $p_2 \leq m_1$. The realization system for the inner loop can be constructed by the transfer from $\left[\begin{smallmatrix} w \\ u \end{smallmatrix}\right]$ to $\left[\begin{smallmatrix} z \\ y \end{smallmatrix}\right]$ as follows:

$$\begin{bmatrix} \dot{x} \\ \hline z \\ \hline y \end{bmatrix} = \left[\begin{array}{c:c:c} A & B_1 & B_2 \\ \hdashline C_1 & D_{11} & D_{12} \\ \hdashline C_2 & D_{21} & D_{22} \end{array}\right] \begin{bmatrix} x \\ \hline w \\ \hline u \end{bmatrix} \tag{24}$$

where

$$[\dot{x} \mid z \mid y]^T = \left[\dot{I}_d \quad \dot{I}_q \mid \varepsilon_d \quad \varepsilon_q \quad z_2 \quad z_3 \mid I_d \quad I_q\right]^T,$$

$$[x \mid z \mid y]^T = \left[I_d \quad I_q \mid E_d \quad E_q \quad I_{dref} \quad I_{qref} \mid V_d \quad V_q\right]^T,$$

$$x = y = \left[I_d \quad I_q\right]^T;\ w = \left[E_d \quad e_q \quad I_{d\_ref} \quad I_{q\_ref}\right]^T;\ u = \left[V_d \quad V_q\right]^T,$$

and $\dot{x} = \begin{bmatrix} \dot{I}_d & \dot{I}_q \end{bmatrix}^T$; $Z = \begin{bmatrix} Z_1 & Z_2 & Z_3 \end{bmatrix}^T$ such as $Z_1 = \begin{bmatrix} \varepsilon_d & \varepsilon_q \end{bmatrix}^T$.

Based on Equation (24), the state space model can be written as follows:

$$\left[\begin{array}{c|c|c} A & B_1 & B_2 \\ \hline C_1 & D_{11} & D_{12} \\ \hline C_2 & D_{21} & D_{22} \end{array}\right] = \left[\begin{array}{cc|cccc|cc} -R/L & \omega & 1/L & 0 & 0 & 0 & -1/L & 0 \\ -\omega & -R/L & 0 & 1/L & 0 & 0 & 0 & -1/L \\ \hline -1 & 0 & 0 & 0 & 1 & 0 & 0 & 0 \\ 0 & -1 & 0 & 0 & 0 & 1 & 0 & 0 \\ 0 & 0 & 0 & 0 & 0 & 0 & 1 & 0 \\ 0 & 0 & 0 & 0 & 0 & 0 & 0 & 1 \\ \hline 1 & 0 & 0 & 0 & 0 & 0 & 0 & 0 \\ 0 & 1 & 0 & 0 & 0 & 0 & 0 & 0 \end{array}\right]. \quad (25)$$

In the same way, the state model for the outer loop is constructed from the nominal plant given previously with different selected weighting functions $Wi(s)$.

4.2. Weight Functions Selection for H∞ Controllers

The weighting functions W_1, W_2 and W_3 are designed to force the closed-loop response to meet system specifications. W_1 is used for error tracking performance. W_1 must be large inside the control bandwidth to obtain small sensitivity S. W_1 is chosen to be a low pass filter in order to reject the external disturbance. W_2 is chosen to ensure the robust performance of the outputs even under disturbed conditions. To limit control effort in a particular frequency band, increase the magnitude of W_2 in this frequency band to obtain small KS requires a small open-loop gain normally in a high frequency range. For noise attenuation, W_3 is chosen outside the control bandwidth to obtain small complementary sensitivity T. W_3 is chosen as a constant and as small as possible, to make sure the matrix D_{12} in generalized plant is full rank, required by the $H\infty$ control.

In this work, the controllers with different weighting functions W_1, W_2 and W_3 were designed using the MATLAB robust control Toolbox. The respective weighting functions are given in Table 1. The resulting $\|Tzw\| = \gamma$ demonstrates the satisfaction of the criterion of a minimum $H\infty$ norm bound.

Table 1. Weight functions selection and γ criterion value.

Loop	Weight Functions $Wi(s)$	$\|Tzw\|$
Inner loop	$W_1(s) = \frac{560s+8.57}{800s+0.01071}$ $W_2(s) = \frac{800s+0.01071}{560s+8.57}$ $W_3(S) = 0.001$	γ = 0.707038
Outer loop	$W_1(s) = \frac{807.5s+1820}{950s+1.916}$ $W_2(s) = \frac{0.2s+200}{s+1000}$ $W_3(s) = 0.0$	γ = 0.858063

The weights assigned by the algorithm for the two controllers are shown in Figures 4 and 5. From Table 1, the two the controllers can be reduced after cancelling poles and zeros, and for the best result, the function 'balreal' in MATLAB can be used. Finally, reduced-order controllers can be obtained as follows:

$$\begin{cases} K_c(s) = \frac{0.19856(s+0.03)}{s+3.903} \\ K_v(s) = \frac{14.3723(s+3.637)}{s+9751} \end{cases} \quad (26)$$

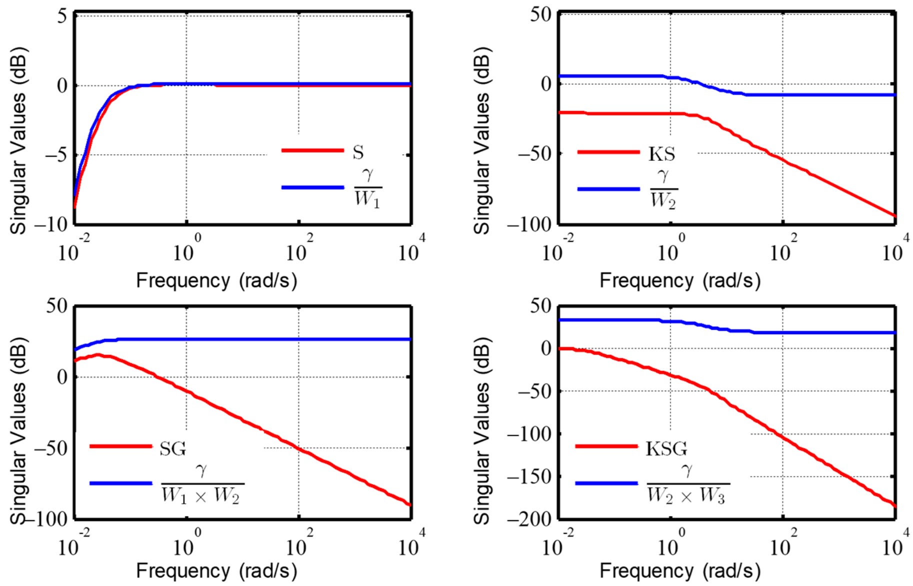

Figure 4. Graphical performances of closed inner loop and weighting functions.

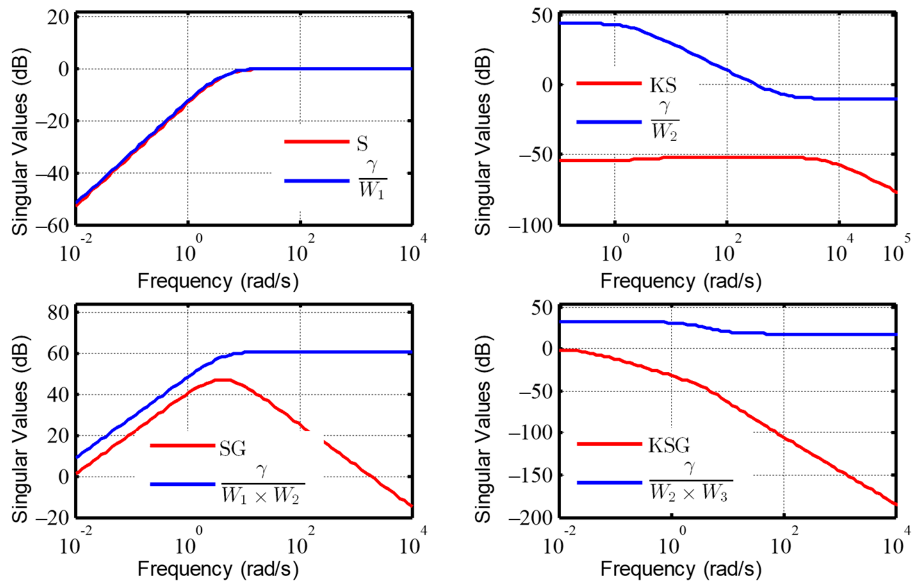

Figure 5. Graphical performances of closed outer loop responses and weighting functions.

For digital implementation purposes, the reduced-order controllers from (26) are discretized using the c2d command in MATLAB. The discretization method used is Tustin with a sampling time of 100 µs.

4.3. Stability and Robustness Performance Analysis

The fundamental requirements of the robust behavior of a closed loop is to ensure two conditions, $\|W_1(s)S(s)\|_\infty < \gamma$ for nominal stability performance and $\|W_2(s)KS(s)\|_\infty < \gamma$ for robust stability. These two conditions can be verified by computing $\|Tzw\|_\infty$ of the closed-loop system and comparing it with performance criterion γ (see Table 1).

To investigate these conditions, the singular value plots of the sensitivity functions and complementary sensitivity functions *KS* of the closed-loop system are presented in Figures 4 and 5, for the inner and outer loops, respectively. Figures 4 and 5 demonstrate that both conditions are satisfied, as the frequency response of each function *S* and *KS* is constrained by the corresponding weights. This observation holds true for *SG* and *KSG* as well. Thus, the criterion in Equation (21) is fully satisfied for both the inner and outer loops. Consequently, the proposed control scheme achieves the desired control performance.

5. Experimental Results

To evaluate the performances of the designed cascaded $H\infty$ controller, an experimental setup has been prepared, as shown in Figure 6. The proposed strategy, illustrated in Figure 3, is implemented on a dSPACE control prototyping system. The grid-side stage consists of a three-phase generator controlled to provide a three-phase AC supply of (80 V, 50 Hz). The grid-side generator is connected to a three-phase SEMIKRON converter that supplies a DC resistive load. The experimental system parameters are given in Table 2. Three tests are realized to evaluate the proposed control in terms of reference tracking and disturbances rejection performances under load transient and unbalanced grid voltage.

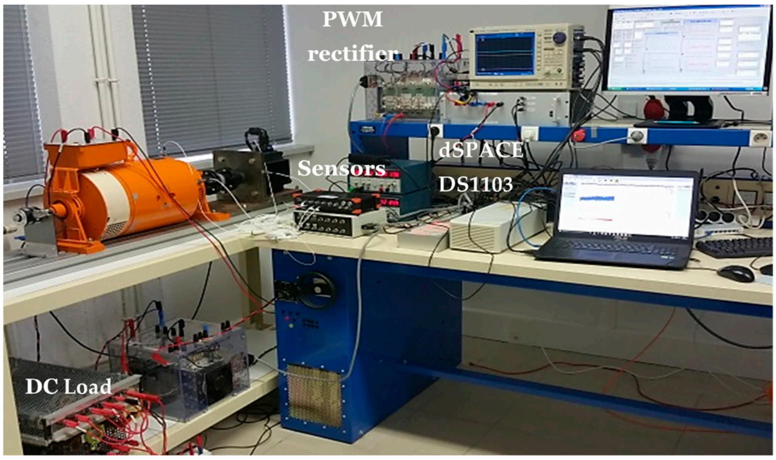

Figure 6. Experimental test setup.

Table 2. System parameters.

Parameters Description	Value
Grid frequency	50 Hz
Grid rms voltage	80 V
Filter resistance R	0.1 Ω
Filter inductance L	10 mH
DC-link capacitor C	1100 µF
Sampling time T_s	100 µs
Switching frequency f_w	5 kHz

5.1. Tracking Performance

In this test, the tracking performances of the outer voltage loop are evaluated under DC voltage reference step change. The DC voltage reference is changed from 300 V to 400 V. The DC voltage response, shown in Figure 7a, illustrates that the proposed control strategy allows for accurate DC voltage tracking performances. Figure 7b presents the *abc* line current's component's evolution. The experimental waveforms of grid voltage and the line current of phase "a" denoted (e_a, i_a) are given in Figure 7c, which are in a phase providing a unity power factor even during transient conditions. The direct and quadrature current components I_d and I_q in Figure 7d show that the proposed control provides a good axis decoupling.

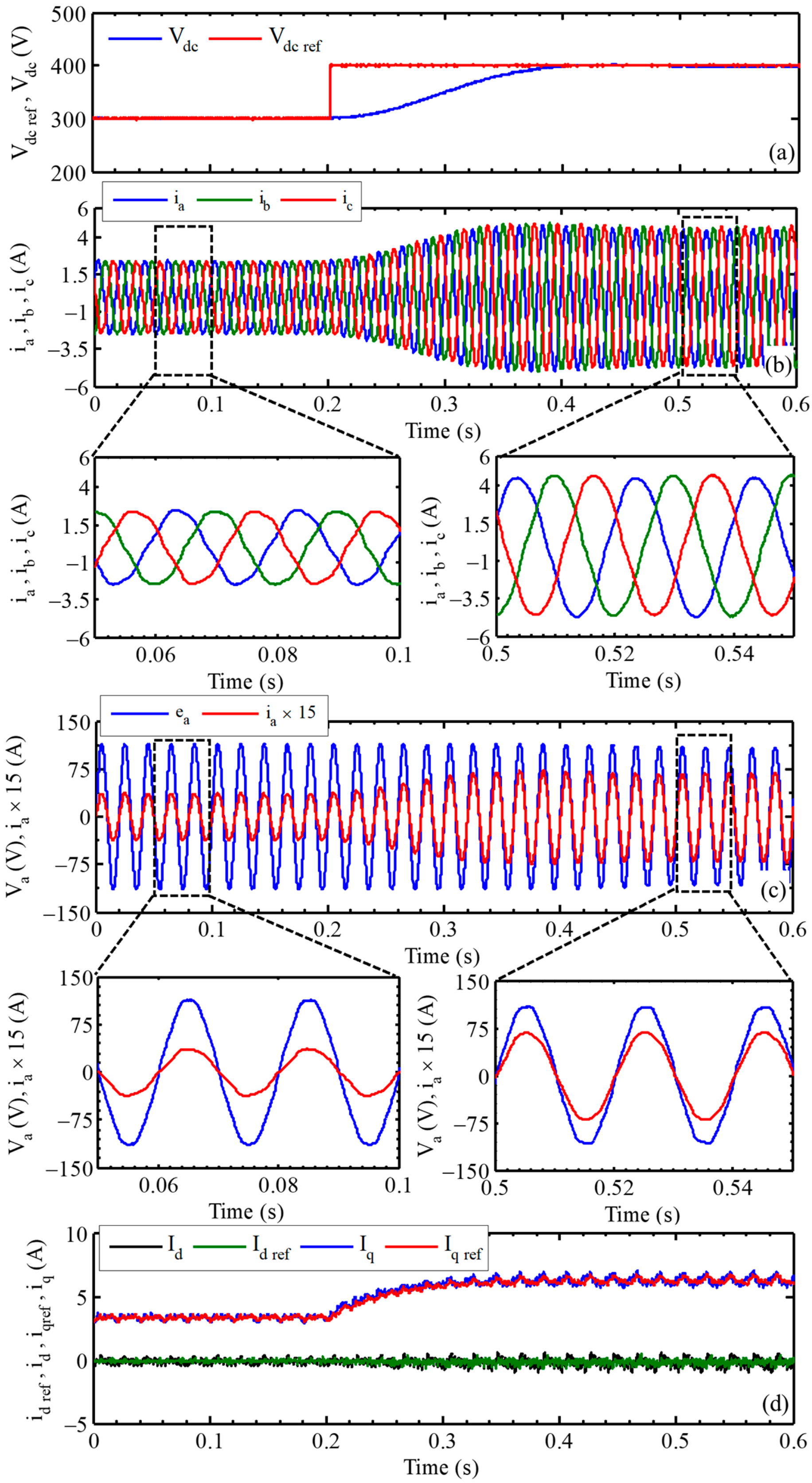

Figure 7. Experimental results under DC-link reference step change from 300 to 400 V: (**a**) DC-link voltages V_{dc} and $V_{dc\ ref}$; (**b**) three-phase grid currents i_{abc}; (**c**) grid current i_a and grid voltage e_a and (**d**) *dq*-axis current components and their references.

5.2. Performances under Transient Loading Conditions

In this test, the proposed control method is evaluated under load step changes. Load step changes from 250 Ω to 110 Ω and then from 110 Ω to 250 Ω are considered. The obtained results are illustrated in Figure 8. Figure 8a highlights when the load changes from 250 Ω to 110 Ω that the DC voltage drop is very low. The DC voltage drop is below 5% from a reference value of 300 V. Figure 8c,f show the corresponding grid voltage and current of phase *a*. This result confirms that the unity power factor is maintained. It can be seen that balanced input currents with low THD are obtained. The DC bus voltage is regulated with suitable load disturbances rejection performances, as shown in Figure 8a,d.

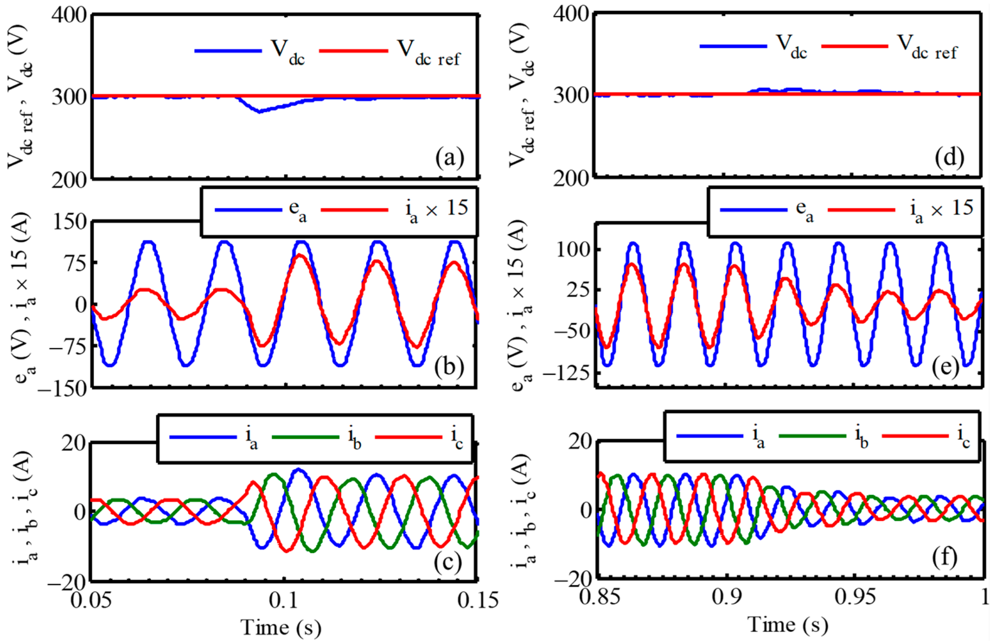

Figure 8. Experimental results under DC load disturbances: (**a**,**d**) DC-link voltage V_{dc} and reference $V_{dc\ ref}$ waveforms; (**b**,**e**) grid current i_a and grid voltage e_a and (**c**,**f**) three-phase grid currents i_{abc}.

5.3. Performance under Unbalanced Grid Voltage

To investigate the proposed control performances under unbalanced conditions, a test under grid voltage unbalance is performed. The grid voltage unbalance is achieved by adding a resistor of 7.2 Ω in series with the passive L filter of phase "*a*". This causes a voltage sag of 10% on phase *a*. The resulting unbalanced grid line currents are illustrated in Figure 9. Figure 9a illustrates that the proposed control strategy allows us to maintain a well-controlled DC bus voltage with good disturbances rejection when the unbalance occurs. Furthermore, Figure 9b shows the grid-phase current i_a and voltage e_a, which are synchronized to maintain the unity power factor. In Figure 9c, the three-phase grid currents waveforms have been illustrated when the imbalanced condition occurs.

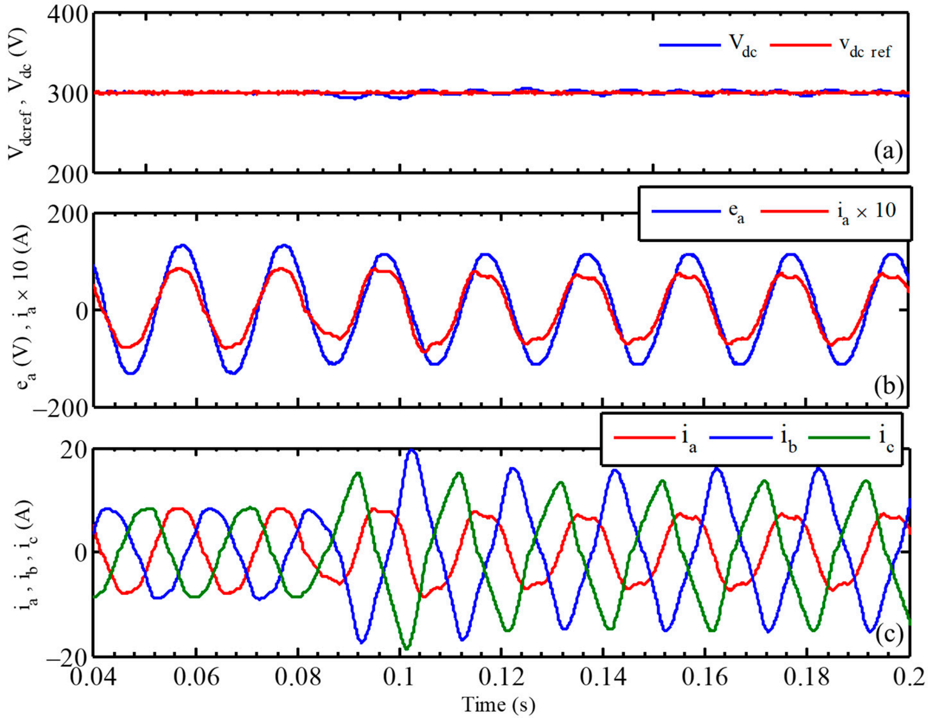

Figure 9. Experimental results under unbalanced grid voltage: (**a**) DC-link voltage V_{dc} and its reference $V_{dc\ ref}$; (**b**) grid current i_a and grid voltage e_a and (**c**) three-phase grid currents i_{abc}.

5.4. Control Performance Comparison

In this experiment, the proposed $H\infty$ control strategy is compared with the conventional PI controller under load disturbances. The results in Figure 10 indicate that the $H\infty$ control strategy surpasses the conventional PI controller. Specifically, the $H\infty$ control strategy shows significantly enhanced dynamic performance, with an improvement of 50%, along with notable reductions in overshoots, also by around 50%. These results highlight the superior abilities of the $H\infty$ control strategy to achieve disturbance rejection and maintain system stability.

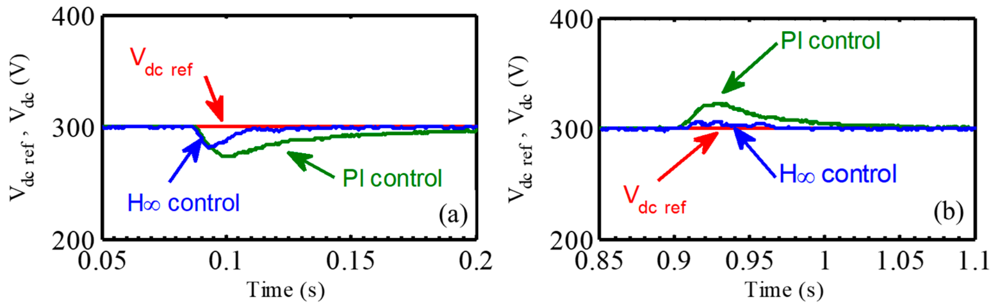

Figure 10. Experimental results of DC-link voltage under load disturbances comparison between conventional PI control and proposed $H\infty$ control: (**a**) load step change from 250 Ω to 110 Ω and (**b**) load step change from 110 Ω to 250 Ω.

6. Conclusions

This article presents a robust $H\infty$ control strategy for grid-connected PWM rectifiers, focusing on disturbance rejection and power quality enhancement. A linearized model of the converter was decomposed into two SISO systems, allowing for a simple controller structure with reduced order and ease of implementation. The resulting two-level control strategy employs cascaded $H\infty$ controllers, ensuring stable DC bus voltage and sinusoidal input currents under various conditions. Extensive experimental tests validated the controller's effectiveness, ensuring accurate tracking and disturbance rejection even under unbalanced grid voltage and load disturbances. Furthermore, the proposed strategy demonstrated its superiority when compared to the PI control method through its ability to minimize overshoots and achieve faster response time.

Although the proposed $H\infty$ control strategy demonstrates robust performance under unbalanced grid conditions, current distortions are still observed. To further enhance the system's performance and maintain sinusoidal currents, future improvements could involve implementing $H\infty$ control algorithms that separately regulate the positive and negative sequence components of the current. Furthermore, utilizing sequence component compensation techniques to actively cancel out the negative sequence components of the current could be beneficial. These approaches could help achieve a more balanced current waveform and reduce harmonic distortion caused by unbalanced grid conditions.

Author Contributions: Conceptualization, N.A.R., A.R. and M.F.B.; methodology, N.A.R., B.B. and M.F.B.; software, N.A.R., M.F.B. and M.A.-A.; validation, N.A.R. and A.D.; investigation, A.R., M.F.B. and B.B.; resources, M.F.B., M.A.-A. and A.D.; writing, N.A.R.; writing—review, N.A.R., A.R. and B.B. All authors have read and agreed to the published version of the manuscript.

Funding: This research received no external funding.

Data Availability Statement: The data presented in this study are available on request from the corresponding author.

Conflicts of Interest: The authors declare no conflicts of interest.

References

1. Ryndzionek, R.; Sienkiewicz, Ł. Evolution of the HVDC Link Connecting Offshore Wind Farms to Onshore Power Systems. *Energies* **2020**, *13*, 1914. [CrossRef]
2. Mesbah, K.; Rahoui, A.; Boukais, B. Neural Network Quadrature Signal Generator-Based Virtual Flux Estimation for Predictive Control of PWM Converters. *IEEE Trans. Ind. Electron.* **2024**, *71*, 4785–4794. [CrossRef]
3. Cittanti, D.; Gregorio, M.; Bossotto, E.; Mandrile, F.; Bojoi, R. Three-Level Unidirectional Rectifiers under Non-Unity Power Factor Operation and Unbalanced Split DC-Link Loading: Analytical and Experimental Assessment. *Energies* **2021**, *14*, 5280. [CrossRef]
4. Rahoui, A.; Mesbah, K.; Boukais, B.; Otmane-Cherif, T. Frequency-Adaptive Neural Network Based Virtual Flux Estimation for Sensorless Control of PWM Converters under Unbalanced Conditions. In Proceedings of the 2020 International Conference on Electrical Engineering (ICEE), Istanbul, Turkey, 25–27 September 2020; pp. 1–6.
5. Kakkar, S.; Maity, T.; Ahuja, R.K.; Walde, P.; Saket, R.K.; Khan, B.; Padmanaban, S. Design and Control of Grid-Connected PWM Rectifiers by Optimizing Fractional Order PI Controller Using Water Cycle Algorithm. *IEEE Access* **2021**, *9*, 125941–125954. [CrossRef]
6. Song, T.; Wang, P.; Zhang, Y.; Gao, F.; Tang, Y.; Pholboon, S. Suppression Method of Current Harmonic for Three-Phase PWM Rectifier in EV Charging System. *IEEE Trans. Veh. Technol.* **2020**, *69*, 9634–9642. [CrossRef]
7. Wang, H.; Wang, S.; Ding, H.; Shi, C.; Jia, D.; Chen, C.; Guerrero, J.M. An Novel Six-Segment Modulation Strategy for Three-Phase Isolated PFC Converter. *Energies* **2022**, *15*, 2598. [CrossRef]
8. Saidi, Y.; Mezouar, A.; Miloud, Y.; Benmahdjoub, M.A. A Robust Control Strategy for Three Phase Voltage t Source PWM Rectifier Connected to a PMSG Wind Energy Conversion System. In Proceedings of the 2018 International Conference on Electrical Sciences and Technologies in Maghreb (CISTEM), Algiers, Algeria, 29–31 October 2018; pp. 1–6.
9. Song, Y.; Jeon, T.; Paek, I.; Dugarjav, B. Design and Validation of Pitch H-Infinity Controller for a Large Wind Turbine. *Energies* **2022**, *15*, 8763. [CrossRef]
10. Djerioui, A.; Houari, A.; Ait-Ahmed, M.; Benkhoris, M.-F.; Chouder, A.; Machmoum, M. Grey Wolf Based Control for Speed Ripple Reduction at Low Speed Operation of PMSM Drives. *ISA Trans.* **2018**, *74*, 111–119. [CrossRef] [PubMed]
11. Viera Díaz, R.I.; Nuñez, C.; Visairo Cruz, N.; Segundo Ramírez, J. A Polynomial Synthesis Approach to Design and Control an LCL-Filter-Based PWM Rectifier with Extended Functions Validated by SIL Simulations. *Energies* **2023**, *16*, 7382. [CrossRef]
12. Suul, J.A.; D'Arco, S.; Rodríguez, P.; Molinas, M. Impedance-compensated Grid Synchronisation for Extending the Stability Range of Weak Grids with Voltage Source Converters. *IET Gener. Transm. Distrib.* **2016**, *10*, 1315–1326. [CrossRef]
13. Wang, J.-H.; Li, H.-D.; Wang, L.-M. Direct Power Control System of Three Phase Boost Type PWM Rectifiers. *Proc. CSEE* **2006**, *26*, 54–60.
14. Yang, D.; Lu, Z.; Hang, N.; Li, G. Novel Quasi Direct Power Control for Three-Phase Voltage-Source PWM Rectifiers with a Fixed Switching Frequency. *Soc. Electr. Eng.* **2011**, *31*, 66–73.
15. Ge, J.; Zhao, Z.; Yuan, L.; Lu, T.; He, F. Direct Power Control Based on Natural Switching Surface for Three-Phase PWM Rectifiers. *IEEE Trans. Power Electron.* **2015**, *30*, 2918–2922. [CrossRef]

16. Zhang, Y.; Qu, C. Direct Power Control of a Pulse Width Modulation Rectifier Using Space Vector Modulation under Unbalanced Grid Voltage. *IEEE Trans. Power Electron.* **2015**, *30*, 5892–5901. [CrossRef]
17. Cho, Y.; Lee, K.-B. Virtual-Flux-Based Predictive Direct Power Control of Three-Phase PWM Rectifiers with Fast Dynamic Response. *IEEE Trans. Power Electron.* **2015**, *31*, 3348–3359. [CrossRef]
18. Kwak, S.; Mun, S. Model Predictive Control Methods to Reduce Common-Mode Voltage for Three-Phase Voltage Source Inverters. *IEEE Trans. Power Electron.* **2015**, *30*, 5019–5035. [CrossRef]
19. Dannehl, J.; Wessels, C.; Fuchs, F. Limitations of Voltage-Oriented PI Current Control of Grid-Connected PWM Rectifiers With Filters. *IEEE Trans. Ind. Electron.* **2009**, *56*, 380–388. [CrossRef]
20. Zeng, Z.; Zheng, W.; Zhao, R.; Zhu, C.; Yuan, Q. Modeling, Modulation, and Control of the Three-Phase Four-Switch PWM Rectifier Under Balanced Voltage. *IEEE Trans. Power Electron.* **2015**, *31*, 4892–4905. [CrossRef]
21. Galecki, A.; Kaszewski, A.; Ufnalski, B.; Grzesiak, L. State Current Controller with Oscillatory Terms for Three-Level Grid-Connected PWM Rectifiers under Distorted Grid Voltage Conditions. In Proceedings of the 2015 17th European Conference on Power Electronics and Applications (EPE'15 ECCE-Europe), Geneva, Switzerland, 8–10 September 2015; p. 10.
22. Campos-Gaona, D.; Peña-Alzola, R.; Ordonez, M. Nonminimum Phase Compensation in VSC-HVDC Systems for Fast Direct Voltage Control. *IEEE Trans. Power Deliv.* **2015**, *30*, 2535–2543. [CrossRef]
23. Jamma, M.; Barara, M.; Akherraz, M.; Enache, B.A. Voltage Oriented Control of Three-Phase PWM Rectifier Using Space Vector Modulation and Input Output Feedback Linearization Theory. In Proceedings of the 2016 8th International Conference on Electronics, Computers and Artificial Intelligence (ECAI), Ploiesti, Romania, 30 June–2 July 2016; pp. 1–8.
24. Akagi, H.; Watanabe, E.H.; Aredes, M. *Instantaneous Power Theory and Applications to Power Conditioning*; Wiley: Hoboken, NJ, USA, 2006; ISBN 978-0-470-10761-4.
25. Trivedi, T.A.; Jadeja, R.; Bhatt, P. A Review on Direct Power Control for Applications to Grid Connected PWM Converters. *Eng. Technol. Appl. Sci. Res.* **2015**, *5*, 841–849. [CrossRef]
26. Longyue, Y.; Jianhua, L.; Chonglin, W. Quasi-Sliding Mode Control of Active Power Filters Based on Exact Feedback Linearization. *Proc. CSEE* **2014**, *34*, 5868–5875.
27. Wang, E.; Huang, S. A Novel Double Closed Loops Control of the Three-Phase Voltage-Sourced PWM Rectifier. *Chin. Soc. Electr. Eng.* **2012**, *32*, 24–30.
28. Si, G.; Zhao, W.; Guo, Z.; Shi, J. A Novel Double Closed Loops Control Strategy of Three-Phase Voltage Source PWM Rectifier with Disturbances. In Proceedings of the 33rd Chinese Control Conference, Nanjing, China, 28–30 July 2014; IEEE: Piscataway, NJ, USA, 2014.
29. Wang, H.; Zhu, C.; Zhang, J.; Zhu, M.; Cai, X. Improved Control for Three-Phase PWM Rectifier Based on Power-Current Model. In Proceedings of the IECON 2020 the 46th Annual Conference of the IEEE Industrial Electronics Society, Singapore, 18–21 October 2020; pp. 3773–3778.
30. Chen, J.; Yao, W.; Zhang, C.-K.; Ren, Y.; Jiang, L. Design of Robust MPPT Controller for Grid-Connected PMSG-Based Wind Turbine via Perturbation Observation Based Nonlinear Adaptive Control. *Renew. Energy* **2019**, *134*, 478–495. [CrossRef]
31. Haneesh, K.M.; Raghunathan, T. Robust Control of DFIG Based Wind Energy System Using an $H\infty$ Controller. *J. Electr. Eng. Technol.* **2021**, *16*, 1693–1707. [CrossRef]
32. Azza, A.; Kherfane, H. Robust Control of Doubly Fed Induction Generator Using Fractional Order Control. *Int. J. Power Electron. Drive Syst. IJPEDS* **2018**, *9*, 1072. [CrossRef]
33. Zhao, K. PWM Rectifier with Fuzzy Sliding Mode Variable Structure Control. *Diangong Jishu Xuebao Trans. China Electrotech. Soc.* **2006**, *21*, 49–53.
34. Lei, T.; Tan, W.; Chen, G.; Kong, D. A Novel Robust Model Predictive Controller for Aerospace Three-Phase PWM Rectifiers. *Energies* **2018**, *11*, 2490. [CrossRef]
35. Johnson, B.B.; Lundstrom, B.R.; Salapaka, S.; Salapaka, M. *Optimal Structures for Voltage Controllers in Inverters*; National Renewable Energy Lab. (NREL): Golden, CO, USA, 2018.
36. Yang, S.; Lei, Q.; Peng, F.Z.; Qian, Z. A Robust Control Scheme for Grid-Connected Voltage-Source Inverters. *IEEE Trans. Ind. Electron.* **2010**, *58*, 202–212. [CrossRef]
37. Weiss, G.; Zhong, Q.-C.; Green, T.C.; Liang, J. $H\infty$ Repetitive Control of DC-AC Converters in Microgrids. *IEEE Trans. Power Electron.* **2004**, *19*, 219–230. [CrossRef]
38. Steenis, J.; Tsakalis, K.; Ayyanar, R. Robust Control of an Islanded Microgrid. In Proceedings of the IECON 2012—38th Annual Conference on IEEE Industrial Electronics Society, Montreal, QC, Canada, 25–28 October 2012; pp. 2447–2451.
39. Steenis, J.; Breazeale, L.; Tsakalis, K.; Ayyanar, R. $H\infty$ and Gain Scheduled $H\infty$ Control for Islanded Microgrids. In Proceedings of the 2013 IEEE Energy Conversion Congress and Exposition, Denver, CO, USA, 15–19 September 2013; pp. 4603–4608.
40. Ibrahim, M.; Ma, L.; Zhao, Y.; Liu, H.; Bo, T. Reliable Current Control for Single-phase Pulse Width Modulation Rectifiers Based on $H\infty$ Loop Shaping Controller. *IET Power Electron.* **2023**, *16*, 2504–2514. [CrossRef]
41. Koch, G.G.; Pinheiro, H.; Maccari, L.A.; Oliveira, R.C.L.F.; Ferreira, A.A.; Montagner, V.F. Robust $H\infty$ control for rejection of voltage disturbances in grid-connected converters. In Proceedings of the 12th IEEE International Conference on Industry Applications, Curitiba, PR, Brazil, 20–23 November 2016; pp. 1–6.
42. Tahami, F.; Ahmadian, H.M.; Moallem, A. Robust $H\infty$ control design for PFC rectifiers. In Proceedings of the 7th International Conference on Power Electronics and Drive Systems, Bangkok, Thailand, 27–30 November 2007; pp. 948–952.

43. Ibrahim, M.M.; Ma, L.; Zhao, Y.; Liu, H. Robust Direct Current Control of Single-Phase PWM Rectifiers Based on a Mixed H. *Stud. Inform. Control* **2023**, *32*, 81–90. [CrossRef]
44. Rahoui, A.; Boukais, B.; Mesbah, K.; Otmane-Cherif, T. Neural Networks Based Frequency Locked Loop for Grid Synchronization under Unbalanced and Distorted Conditions. In Proceedings of the 2020 International Conference on Electrical Engineering (ICEE), Istanbul, Turkey, 25–27 September 2020; pp. 1–5.
45. Doyle, J.; Glover, K.; Khargonekar, P.; Francis, B. State-space solutions to standard h2 and h-infinity control problems. *IEEE Trans. Autom. Control* **1989**, *34*, 831–847. [CrossRef]
46. Zhao, Y.; Ma, L.; Liu, H.; Peng, L. A dual-loop model predictive power control scheme for single-phase PWM rectifiers. In Proceedings of the 42nd IEEE Chinese Control Conference (CCC), Tianjin, China, 24–26 July 2023; pp. 2670–2675.
47. Pérez, J.; Cobreces, S.; Griñó, R.; Sánchez, F.J.R. $H\infty$ current controller for input admittance shaping of VSC-based grid applications. *IEEE Trans. Power Electron.* **2017**, *32*, 3180–3191. [CrossRef]